ORIGINAL ARTICLE

The insensitivity of convective intensity to boundary layer height and boundary layer heterogeneity in radiative-convective equilibrium

Emmanuel Sarbeng[1*] | **Martin S. Singh PhD**[1*]

[1]School of Earth, Atmosphere and Environment, Monash University, Victoria, 3800, Australia.

Correspondence
Emmanuel Sarbeng, School of Earth, Atmosphere and Environment, Monash University, Melbourne, Victoria, 3800, Australia.
Email: emmanuel.sarbeng@monash.edu

Present address
[†]School of Earth, Atmosphere and Environment, Monash University, Melbourne, Victoria, 3800, Australia.

Funding information
Australian Research Council, Centre of Excellence for Climate Extreme, Grant/Award Number: DE190100866 and DP200102954.

Previous modeling studies have come to mixed conclusions as to how changes in different surface properties may affect cloud updraft velocities in seeking to explain observed land-ocean contrasts in convective intensity. Here we show that varying surface Bowen ratio in idealised radiative-convective equilibrium simulations over both homogeneous and heterogeneous surfaces does not result in significant changes to the intensity of convective storms as measured by high percentiles of the updraught velocity distribution. While both a deeper boundary layer and heterogeneity of the surface can lead to a change in the cloud size distribution and consequent changes in cloud entrainment, we find that this only marginally affects the intensity of the strongest updraughts. These results are explained by appealing to a model of convection as a spectrum of entraining plumes. According to this model, updraft strength is primarily sensitive to the width of the distribution of entrainment among the spectrum of plumes. This is because entrainment sets both the profile within cloud updrafts and the mean lapse rate of the troposphere. If cloud sizes are increased, en-

Abbreviations: SBR, surface Bowen ratio; LHF, latent heat flux; SHF, sensible heat flux; RCE, radiative convective equilibrium; RH, relative humidity; CAPE, convective available potential energy.

[*]Equally contributing authors.

trainment is reduced, and this both protects clouds from their unsaturated environment but increases the stability of the troposphere; each of these effects have countervailing influences on cloud updrafts.

KEYWORDS
deep convection, *surface Bowen ratio*, *updraught velocity*, homogeneous surface, heterogeneity surface, entrainment

1 | INTRODUCTION

Multiple observation studies (e.g., Lucas *et al.*, 1994; Christian *et al.*, 2003; Zipser *et al.*, 2006; Liu and Zipser, 2015) using different intensity metrics have argued that convective storms that form over land are substantially deeper and stronger than those that form over the ocean. Common metrics that have been used in assessing the intensity of storms include lightning flash rate (e.g., Zipser *et al.*, 2006), overshooting distances of convective clouds into the stratosphere (e.g., Liu and Zipser, 2005; Hong *et al.*, 2008), and the updraft velocity in convective clouds (e.g., Lucas *et al.*, 1994). For all these measures, continental storms have been shown to be substantially more vigorous than their oceanic counterparts.

To help explain the large land-ocean contrast in storm intensity, Williams and Stanfill (2002) hypothesized a link between the intensity of storms over land and some physical characteristics peculiar to the land surface. Specifically, they highlighted the high boundary layer depth, high aerosol concentration, heterogeneous nature of the land surface, and strong diurnal cycle of temperature as characteristics that plausibly enhance the intensity of storms that form over land. However, a full theoretical understanding of the relative importance of these different surface features remains lacking. In this study, we focus on two of these characteristic features of the land surface, high boundary layer depth and spatial heterogeneity of surface fluxes, to assess their linkage to storm intensity in an idealized radiative-convective equilibrium (RCE) setting using a cloud resolving model.

As a result of the different partitioning between sensible and latent heat fluxes, the boundary layer tends to be substantially deeper over land surfaces compared to over the ocean (Avissar and Schmidt, 1998). A key measure of this partitioning is the surface Bowen ratio (SBR), given by the ratio of the sensible heat flux to the latent heat flux, which has been shown to be closely related to the boundary layer depth over much of the tropics (Kang and Bryan, 2011). Lucas *et al.* (1994) argued that the width of convective clouds scale with the size of boundary layer thermals; therefore, clouds that form over surfaces with higher Bowen ratio are rather wider at birth because the boundary layer is deeper. Such clouds therefore experience less dilution through mixing with the environment, potentially allowing them to achieve higher velocities.

Williams *et al.* (2004), using observations over islands of different sizes, affirmed that variations in boundary layer depth provide a plausible candidate in explaining the land-ocean contrast in storm intensity. A modelling study by Kang (2016) on the diurnal cycle of convective clouds with prescribed surface fluxes showed that afternoon convective storms were wider and more vigorous in cases with high SBR compared to those with low SBR. However, a contrasting study by Hansen and Back (2015) with no imposed diurnal cycle explored the sensitivity of different convective intensity metrics to changes in SBR in both RCE and initial-condition simulations, concluding that varying the boundary layer depth has little to no effect on the strength of convective storms as measured by high-percentile updraft velocity. Hansen and Back (2015) found the argument of deeper boundary layer depth leading to wider clouds

and less entrainment made by some studies (e.g., Williams and Stanfill, 2002; Williams *et al.*, 2005) to be partially true; whereas the deeper boundary layer depth resulted in wider clouds, it did not lead to stronger convection, and the convective entrainment was found to be independent of the boundary layer depth.

The contrasting findings in the different studies may be attributed to a number of reasons including the experimental design, the numerical model used, and the metrics used in assessing the strength of the convective storms. It is also important to note that most studies that show intense storms over surfaces with a deeper boundary layer have an imposed diurnal cycle in their experimental design, the coupled effect of these two surface features (high SBR and strong diurnal cycle of temperature) may be the reason for the enhanced convection over land in these studies, and possibly the reason for the difference in their results from studies that only consider the boundary layer depth of the land surface.

Heterogeneity of the land surface has also been suggested as a surface feature with potential control on the intensity of storms that form over land (e.g., Hansen and Back, 2015; Romps *et al.*, 2018). For example, a number of studies have investigated the acceleration of the transition from shallow clouds to deep convective clouds over a heterogeneous land surface compared to a homogenous one. However, these studies do not focus on the intensity of deep convective clouds once they reach full maturity. A key goal in this study is therefore to understand how the intensity of deep convective clouds respond to a defined heterogeneous land surface within a radiative-convective equilibrium framework.

The land surface is made of different orographic features and vegetative cover, producing spatial differences in soil wetness and surface roughness and introducing heterogeneity at a variety of scales (Avissar and Schmidt, 1998). The nonuniform heating of the heterogeneous land surface results in spatial differences in surface fluxes which affect the state of the atmospheric boundary layer (Rieck *et al.*, 2014; Wu *et al.*, 2015b). For example, spatially varying soil moisture may produce patches of low (dry patch) and high (wet patch) evaporative fractions, which ultimately lead to different partitioning between the sensible heat flux (SHF) and latent heat flux (LHF) over the patches.

High resolution modelling studies on the effect of land surface heterogeneity on convection (e.g., Giorgi *et al.*, 1997; Avissar and Schmidt, 1998; Kang and Bryan, 2011; Rochetin *et al.*, 2017; Lee *et al.*, 2018; Knist *et al.*, 2019) have found that surface heterogeneity induces mesoscale circulations that result in enhanced updraft velocity and faster transitioning of shallow to deep clouds mainly over regions with high SHF (dry patch). Lee *et al.* (2018) performed large-eddy simulations (LES) in which heterogeneity was introduced through a prescribed spatially varying SHF and found that shallow clouds that were able to transition into deep clouds formed mainly over the dry patches. They attributed this to the secondary circulation induced by the heterogeneity of the domain. They found that only simulations with heterogeneity patch size greater than 5 km could induced such circulations, highlighting the importance of the spatial scale of heterogeneity. A similar study by Rieck *et al.* (2014) also showed that shallow clouds transition faster into deep clouds over heterogeneous surfaces with large patch size compared to those over homogeneous surfaces. However, similar cloud size distributions were found regardless of the heterogeneity patch size simulated. While the above studies demonstrate the effect of heterogeneity of surface fluxes on the initiation and transitioning of clouds, there are still outstanding questions as to whether and how a heterogeneous surface affects the peak intensity of storms.

Here we perform series of relatively high resolution simulations aimed at assessing the effects of varying SBR over both a homogeneous and heterogeneous domain on the intensity of storms as measured by high percentile updraught velocity. We vary the SBR by altering the moisture availability of the surface, guided by the available literature and hypotheses on land surface features and storm intensity. For each idealized RCE simulation, we are interested in finding the relationship between the SBR, the cloud size distribution, the convective available potential energy (CAPE), the dilution of the cloud core by environmental air (entrainment) and the resulting convective strength. We also run simulations for different heterogeneity patch sizes to assess whether the intensity of storms is affected

by the size of the heterogeneous surface.

Although simulations of RCE present their own limitations, RCE has been shown to be an ideal tool for estimating convective processes and the sensitivity of deep clouds to specific surface features (Rochetin *et al.*, 2014). The idea here is to test the response of the intensity of convective storms to different surface features. Our approach therefore does not seek to replicate real-world convection scenarios.

The rest of the paper is structured as follows; we first describe the model setup and simulations (section 2). We then present results for the intensity of updrafts and its relationship to the cloud size distribution (section 3). We analyze the linkages between the surface moisture availability and its heterogeneity and large scale parameters like CAPE by applying a simple entraining plume representation of convection (Section 4). We finally recap the main findings and present conclusions (section 5).

2 | MODEL DESCRIPTION AND SETUP

We run simulations to radiative-convective equilibrium (RCE) using version 6.11.2 of the System For Atmospheric Modeling (SAM; Khairoutdinov and Randall, 2003). All simulations are conducted with a horizontal grid spacing of 500 m over a doubly periodic domain of 128 km $\times$ 128 km and 64 vertical levels. The simulations are non-rotational and have no imposed background flow. Subgrid-scale turbulence and microphysics are parameterised using a 1.5 order TKE closure and Morrison two-moment microphysics scheme, respectively. Surface fluxes are evaluated using bulk aerodynamic formulas with transfer coefficients calculated using Monin-Obukov similarity theory. These formulas are altered to introduce variations in the moisture availability as described below.
Our simulations utilise the fully interactive Rapid Radiative Transfer Model scheme (RRTM; Clough *et al.*, 2005). There is no diurnal cycle in our simulations, we assume a constant solar flux of 551 W m^{-2} and a zenith angle of 42.05°. All simulations are run in 3D for a total of 50 days with statistics sampled at 30 minute intervals. Data from the last 20 days of the simulations are used in all analysis.

2.1 | Altering the available surface moisture

The first set of simulations follow the approach of Hansen and Back (2015) to assess the effect of boundary layer depth on the intensity of convective storms over a homogeneous surface. An important control of the tropical boundary layer depth is the Bowen ratio, with the land surface generally having a higher Bowen ratio and consequently a deeper boundary layer than the ocean surface.

Here we alter the Bowen ratio in our RCE simulations by the introduction of an evaporative conductance parameter (α) into the bulk equation for the latent heat flux. The latent heat flux (LHF) is given by:

$$LHF = \alpha C_e |v| (q_s - q), \tag{1}$$

where C_e is the bulk transfer coefficient, $|v|$ is the magnitude of wind speed, q_s is the surface saturated specific humidity, and q is the near-surface specific humidity. The α value so introduced increases or decreases the latent heat flux; a higher α value results in higher latent heat flux and vice versa.

2.2 | Simulations

For our control simulation, we use an α value of 1 which represents a simulation with higher latent heat flux (low SBR) typical of a tropical ocean-like surface (hereafter, HOM). For our homogeneous land-like simulation (hereafter, HOML), we use an α value of 0.25.

Extending the work of Hansen and Back (2015), we also run simulations over heterogeneous land-like domains to assess the impact of horizontal gradients of moisture availability and SBR on the intensity of convective storms. Heterogeneity is imposed over our domain in a checkerboard pattern with alternating α values of 1 and 0.25 to represent low SBR (cool and wet patch) and high SBR (warm and dry patch) regions respectively. We run four different simulations HET8, HET16, HET32 and HET64 to represent simulations over a heterogeneous land-like surface with patch sizes of side length 8 km, 16 km, 32 km and 64 km, respectively. For all land-like simulations, we devise an iterative approach to maintain a similar free-tropospheric temperature profile in each simulation, as described below.

2.3 | Maintaining a similar free-tropospheric temperature profile

As noted by Hansen and Back (2015), lowering the α value to differentiate simulations over ocean and land surfaces result in cooling of the lower free troposphere and therefore requires a corresponding increment of the SST to ensure a relatively similar free-tropospheric temperature profile in the simulations. This is important because the free-tropospheric temperature is known to influence the intensity of storms (Singh and O'Gorman, 2015), and the tropics is known to have a relatively weak horizontal gradient in free-tropospheric temperature. A similar free-tropospheric temperature in all simulations is therefore achieved through an iterative process that works to nudge the mean SST at every time step until the lower-tropospheric temperature in the simulation is close to that of a reference temperature profile.

First, our control simulation HOM is run with a fixed SST of 300K. The time and domain-mean temperature profile of this simulation is then used as the reference profile for HOML and the heterogeneous simulations. Next, we run the land-like simulations with a modified slab-ocean lower boundary condition. Specifically, the SST at each grid point is governed by a local energy balance equation given by

$$c_{pl} h \frac{dSST}{dt} = F'_{\text{net}} - LHF' - SHF' + \delta T \tag{2}$$

Here F_{net} is the net radiative flux into the surface, c_{pl} is the specific heat capacity of liquid water, and h is the depth of the slab. The primes refer to anomalies from the domain mean such that the energy imbalance over the entire domain does not cause any change in the domain-mean SST. Rather, the evolution of the domain-mean SST is governed by the final term, which is defined by a temperature increment δT. The temperature increment is given by

$$\delta T = \frac{(\int_{2km}^{6km} \overline{T} - \int_{2km}^{6km} T_t)}{H\tau} \tag{3}$$

where $\overline{T}$ is the mean reference temperature profile from our control simulation, T_t is the temperature profile for the current simulation at every time step, H = 4 km and τ = 6 hours. The above procedure allows the surface to locally respond to energy imbalances to produce gradients in surface temperature, but it decouples the mean SST from the surface energy balance. Instead, the domain-mean SST evolves in such a way that the land-like simulations develop a similar temperature in the lower free troposphere (between 2 and 6 km) as HOM. In this way the free-tropospheric temperature remains almost equal between our low and high Bowen ratio cases. After implementing the

free troposphere warming approach discussed above, the mean surface temperature for the homogeneous land-like simulation (HOML) was found to be 304.5K and a mean SST value of 301.7K was obtained for all the heterogeneous simulations. This results in a free-tropospheric temperature similar to that of HOM for all cases as shown in Figure 1.

3 | RESULTS

3.1 | Boundary layer depth and cloud organization

As shown in Table 1, altering the moisture availability results in different boundary layer depths (as measured by the height of the cloud base) for the different simulations. Considering the two homogeneous cases, the land-like (HOML) simulation with an α value of 0.25 results in a relatively deeper boundary layer of approximately 1300 m, more than twice the boundary layer depth of the control case (HOM). The SBR for the HOML and HOM cases are 0.32 and 0.09 respectively. The influence of the surface fluxes on the near surface moisture is clearly shown in the values of relative humidity at the first model level. The HOM case has a relatively wet surface with a relative humidity of 76% compared to the relatively dry HOML case with a mean near-surface relative humidity of 52%. For the heterogeneous simulations, the boundary layer depth, SBR and surface relative humidity are all approximately independent of patch size, and their values fall in-between those of HOM and HOML. The similar domain-and-time average structure of variables within the boundary layer in the heterogeneous cases agree with earlier findings of Liu *et al.* (2017) who concluded that domain-and-time averages of state variables and fluxes in the boundary layer are insensitive to the heterogeneity of the land surface.

Figure 2 shows the time-mean distribution and organisation of cloud water path (CWP) in each simulation. This provides a sense of the arrangement of clouds over both the homogeneous and heterogeneous surfaces. Clouds appear to form relatively randomly in simulations with a homogeneous surface (HOM and HOML), with little evidence of organization or aggregation behaviour that is seen in some previous RCE simulation studies (e.g: Bretherton *et al.*, 2005). For the heterogeneous cases (HET8, HET16, HET32, HET64), clouds predominantly form over regions with low evaporative fraction (dry patches), consistent with earlier findings (e.g., Kang and Bryan, 2011; Rieck *et al.*, 2014; Wu *et al.*, 2015a; Lee *et al.*, 2018).

This may be explained by appealing to the mesoscale secondary circulation mechanism reported in various studies; the horizontal gradients in SHF over the heterogeneous domains result in horizontal pressure gradients which lead to the advection of moisture from the cool and wet patches to the warm and dry patches (Giorgi *et al.*, 1997). The so-induced circulation results in vertical transport of moisture and subsequent cloud formation over the dry patches.

3.2 | Updraught Velocities

Figure 3 shows the updraught strength of the simulations as measured by the 99.99th percentile vertical velocity (Figure 3a) and the mean in-cloud vertical velocity (Figure 3b) at each vertical level. Variations in the surface conditions have a very weak effect on the intensity of storms. For both intensity metrics considered, there appears to be no invigoration of the storms with boundary layer depth. This agrees with similar findings by Rieck *et al.* (2014) and Hansen and Back (2015). Indeed, our simulations show an in-cloud vertical velocity of about 1 m s^{-1} higher over the ocean-like (HOM) simulation at the 500 hPa level compared to the land-like simulation (HOML).

There is no definite pattern in our heterogenous simulations to support the hypothesis that updraught velocity over a heterogenous surface increases with increasing heterogeneity patch size. Again, there is no significant difference in the updraught velocities between the homogeneous simulations and the heterogeneous simulations. Hence, the

hypothesis that a heterogeneous surface could invigorate storms is not supported in our idealised simulations when the entire domain is considered.

3.3 | Cloud Sizes

We explore our results further by assessing the sizes of clouds from the simulations. Differences in cloud sizes, driven by variations in boundary layer depth, provides one possible mechanism by which the SBR may influence the intensity of storms (Williams *et al.*, 2005). It is argued that the deeper boundary layer over land leads to larger cloud sizes which are less affected by entrainment therefore achieving higher buoyancies. To estimate cloud size, we define cloudy grid points as those with a non-precipitating condensate value of 0.01 g kg^{-1} or greater. We then form clusters of cloudy points by taking 8-connected regions of clouds that occupy 8 grid-points or more. The size of the cloud is then given by the horizontal area of a given cluster.

Figure 4 shows the distribution of cloud area between 2 and 5 km from each simulation. For the homogeneous simulations, the land-like case (HOML) exhibits a shift in the distribution from small clouds (< 5 km^2) to larger clouds when compared to the ocean-like case (HOM).

Considering the heterogeneous simulations, cloud area tends to increase with the heterogeneity patch size; the largest clouds are twice as large in the simulation with largest patch size (HET64) compared to the simulation with the smallest patch size (HET8). Although the cloud areas calculated in the heterogeneous simulations increase with patch size, the difference in cloud area does not necessarily scale with the difference in patch sizes. Furthermore, from our simulations, there is no evidence to support the notion that clouds that form over heterogeneous surfaces are larger than those that form over homogeneous surfaces. Indeed at the 99.99th percentile (not shown), the largest clouds are over the homogeneous land-like case (HOML) albeit marginally wider than the heterogeneous case with large patch size (HET64).

4 | PHYSICAL MECHANISMS

We have seen that neither boundary layer depth variations nor heterogeneity of surface moisture availability result in substantial invigoration of convective storms in RCE despite having some effect on the size distribution of clouds. We now attempt to understand the physical basis for this lack of sensitivity. Specifically, we examine the effect of convective entrainment on our simulations. Williams and Stanfill (2002) hypothesized that wider clouds would experience less dilution from entrainment, thereby achieving higher updraft speeds. However, Singh and O'Gorman (2013) found that, in RCE, convective entrainment also plays a role in setting the tropospheric lapse rate. They introduced a theoretical model for the lapse rate based on a neutrally buoyant entraining plume that implies that CAPE increases with the entrainment rate. Extending this work, Singh and O'Gorman (2015) developed a two-plume model, in which the second plume represents the most intense updrafts, to account for changes in updraft speeds with warming in RCE. According to this two-plume model, cloud updraft velocities are determined by a measure of the width of the distribution of entrainment rates experienced by different updrafts. Here, we examine to what extent these ideas are able to explain the results of our simulations with varying boundary-layer depth and varying surface heterogeneity.

4.1 | Interpretation using spectrum of entraining plumes

To begin, we interpret our simulation results within a framework in which convection is represented as a spectrum of entraining plumes. To do so, we consider the distribution of moist static energy (MSE) at each vertical level within the simulations. Here the MSE h is defined

$$h = c_p T + g z + L_v q, \tag{4}$$

where, c_p is the isobaric specific heat capacity of dry air, T is the temperature, g is gravity, z is the height above the surface, L_v is the latent heat of vaporization, and q is the specific humidity of water vapor. As shown in Figure 5, at most levels within the free troposphere, the vast bulk of the MSE distribution is concentrated close to the mean MSE $\overline{h}$, but there are some gridpoints that have relatively high MSE values, far in excess of $\overline{h}$ or even the mean saturation MSE $\overline{h}^*$ at that level, and closer to the typical MSE values in the boundary layer. Since the MSE is approximately conserved for adiabatic motions, we may interpret these high-percentile MSE values as occurring in air that has experienced a relatively low amount of entrainment as it has risen through clouds from the boundary layer.

To quantify the entrainment experienced by air parcels with different values of MSE, we define a set of plumes with moist static energy h_p governed by the equation

$$\frac{dh_p}{dz} = -\epsilon(h_p - \overline{h}) \tag{5}$$

with lower boundary conditions given by the mean MSE at the lowest model level, and with a variety of different entrainment rates ϵ. For simplicity, we use constant values of the entrainment rate in the free troposphere and set $\epsilon = 0$ within the boundary layer. We may now define an effective entrainment rate for air parcels within the free troposphere based on the value of ϵ that gives $h_p(z;\epsilon) = h(z)$ at a given height z. The value of $h_p(z;\epsilon)$ for a range of entrainment rates is shown by the thin black lines on Figure 5.

Examination of Figue 5 reveals that different simulations have differing distributions of the effective entrainment rate. For example, the 99.99th percentile of the MSE distribution has an effective entrainment rate of roughly 0.2 km^{-1} over the lower troposphere in HOM, whereas for the same percentile the effective entrainment rate is closer to 0.15 km^{-1} in HET64. The variation in SBR, and the associated variations in boundary-layer depth and cloud size, appear to induce a change in the distribution of entrainment across the simulations. Why does this not lead to larger changes in updraught velocity?

To answer this question, we note that cloud buoyancy depends on the density of a cloud compared to its environment, which is approximately a monotonic function of the difference $h^* - \overline{h}^*$, where h^* is the in-cloud saturation MSE. Cloud buoyancy therefore depends not only on high-percentiles of the MSE distribution but also the saturation MSE of the mean profile, and a model for both is needed to understand convective intensity.

Singh and O'Gorman (2013) provided a model for the mean saturation MSE $\overline{h}^*$ in RCE based on the assumption that convection remains neutrally buoyant relative to an entraining plume initialized within the boundary layer. However, this zero-buoyancy plume model cannot be used to estimate convective intensity, because it neglects cloud buoyancy entirely and assumes $h^* - \overline{h}^* = 0$. To remedy this, Zhou and Xie (2019) extended the zero-buoyancy plume model to a spectrum of plumes, with $\overline{h}^*$ set by the plume that becomes neutrally buoyant at level z. Here we follow Singh and O'Gorman (2015) and consider the simplest possible spectral approach that considers only two entrain-

ing plumes. In this two-plume model, one plume represents the bulk of the convective mass flux; the mean profile is assumed to be neutrally buoyant to this plume with entrainment rate ϵ_{mean}. The second plume represents high-percentile updrafts and has a correspondingly lower entrainment rate.

We estimate these two entrainment rates for each of our simulations at a mid-tropospheric level $z_m = 5$ km. The entrainment rate ϵ_{mean} is given by the entrainment rate such that $h_p(z_m; \epsilon_{\text{mean}}) = \overline{h}^*(z_m)$. This may be visualized as the entrainment rate for which the thin black curves on Fig. 5 intersect the saturated MSE (thick black) curve at $z_m = 5$ km. The entrainment rate of high-percentile updrafts $\epsilon_{99.99}$ is given by the entrainment rate such that $h_p(z_m; \epsilon_{99.99}) = h_{99.99}(z_m)$, where $h_{99.99}$ is the 99.99th percentile MSE. This may be visualized as the intersection of the thin black curves on Fig. 5 and the boundary separating yellow and orange at the 5 km level. It is important to note that non-entraining plumes are essentially absent in our simulations, since even for the highest MSE percentiles, the effective entrainment rates remain substantial.

4.2 | Cloud size and entrainment

Having diagnosed the bulk entrainment rate ϵ_{mean} and the high-precentile entrainment rate $\epsilon_{99.99}$, we may now evaluate how they vary across the simulations. As shown in Figure 6c, both ϵ_{mean} and $\epsilon_{99.99}$ decrease with increasing patch size in the heterogeneous cases. The bulk entrainment of HET8 is roughly double that of HET64. On the other hand, for the homogenous cases, ϵ_{mean} is slightly larger in HOML compared to HOM, while $\epsilon_{99.99}$ has the opposite trend.

Since the size of clouds increases with patch size, the entrainment variations in the heterogenous cases are consistent with the hypothesis that wider clouds are more protected from the environment and entrain less (Williams and Stanfill, 2002). For example, in the heterogenous cases, the bulk entrainment rate ϵ_{mean} monotonically decreases with an increase in the size of clouds, as measured by the 99.9th percentile (Figure 6d). In the homogenous cases, the relationship between cloud size and entrainment depends on the part of the cloud-size distribution that is examined. HOML has fewer moderate sized clouds (~ 5 km^2), but a larger number of large clouds in excess of 10 km^2. This is consistent with the hypothesised relationship between cloud size and entrainment if one supposes that the entrainment rate for the bulk of the convective mass flux is set by the more numerous but relatively small sized clouds, while the entrainment rate of the most intense updrafts is set by the largest clouds.

4.3 | Effects of entrainment on CAPE and updraught velocities

According to the two-plume model of Singh and O'Gorman (2015), the entrainment rates ϵ_{mean} and $\epsilon_{99.99}$ respectively control the lapse rate and updraft distribution of convection in RCE. Specifically, for a constant mean temperature and depth of troposphere, the two-plume model suggests that the convective available potential energy (CAPE) scales as

$$CAPE \sim \epsilon_{\text{mean}}(1 - RH), \tag{6}$$

where RH is a measure of the tropospheric relative humidity. The equation above is based on the fact that the deviation of the lapse rate from that of a moist adiabat is due to the mixing of dry air into clouds as they rise toward the tropopause. The effect of this mixing is proportional to the entrainment rate ϵ_{mean} and the subsaturation of the free troposphere (see Equation (4) of Singh and O'Gorman, 2013).

To test the scaling (6), we diagnose CAPE in each simulation as the integral of the positive buoyancy of a parcel lifted pseudoadiabatically and initialised with the mean temperature and specific humidity at the lifting condensation level in each simulation. Ice processes are treated with a mixed-phase range between 233.15 and 273.15 K. The

parcel buoyancy is then calculated with respect to the domain-and time-mean virtual temperature.

In our heterogenous simulations, the CAPE, ϵ_{mean}, and the lower tropospheric RH all decrease with increasing patch size (Figure 6). Interpreting this through the lens of the two-plume model, this suggests that changes in relative humidity and entrainment have opposite influences on the CAPE, although the effect of changing entrainment wins out, causing CAPE to decrease with patch size. Indeed, as shown in table 2, the value of $\epsilon_{\text{mean}}(1 - RH_{23})$ where RH_{23} is the mean relative humidity between 2 and 3 km does decrease with patch size, although the fractional decrease is smaller than that of the CAPE.

In the homogenous simulations, the CAPE decreases considerably as the SBR increases, but the entrainment rate and relative humidity change only marginally and in ways that would affect the scaling for CAPE in opposite directions. The two-plume model therefore does not capture the behaviour of the CAPE in response to a change in boundary layer depth. We do not at present have a full explanation for this result, but we speculate that changing the depth of the boundary layer affects turbulence characteristics within it, thereby affecting the properties of air parcels that leave the boundary layer in clouds. Our calculation of CAPE, however, neglects such effects; it assumes that the relevant parcel has the mean properties of the lowest model level in all cases.

Finally, we turn to convective intensity itself. According to the two-plume model, the buoyancy within the strongest updrafts depends on the difference between the entrainment rate relevant to the bulk of convection and the entrainment rate relevant to high-percentile updrafts. Singh and O'Gorman (2015) derive an equation for the temperature excess within such strong updrafts [see their Equation (10)]. Based on this, we may write a scaling relation for updraft velocity given by

$$w^2 \sim \delta\epsilon(1 - RH). \tag{7}$$

Here w is a measure of updraft strength and $\delta\epsilon = \epsilon_{\text{mean}} - \epsilon_{99.99}$. This scaling relation assumes that the free tropospheric temperature and the depth of convection are invariant; owing to our free-tropospheric temperature relaxation approach, these are good approximation in our simulations.

Consistent with the results for vertical velocity presented in the previous section, the scaling (Equation 7) varies little across both the homogenous and heterogenous simulations (table 2) except in the case of HET64. This is despite variations in the entrainment rates ϵ_{mean} and $\epsilon_{99.99}$ and the subsaturation $(1 - RH_{23})$ of the order of 100%. The reason for this is two-fold. Firstly, in the heterogenous simulations, ϵ_{mean} and $\epsilon_{99.99}$ vary together, and so their difference has relatively small variations. As the patch size increases, all clouds become larger, reducing the amount of entrainment into clouds. On its own, this would act to strengthen the strongest updrafts. However, because the lapse rate itself is dependent on entrainment, the atmosphere becomes more stable, reducing the instability. These two effects offset each other and their effect on the updraft speed. Notwithstanding the above offsetting effect, the simulations do exhibit some changes in the entrainment difference $\delta\epsilon$, particularly for the homogenous cases. However, we also find that the environmental relative humidity tends to vary in such a way as to offset some of these changes, resulting in weak changes in the vertical velocity scaling across all simulations.

The scaling (Equation 7) provides a mechanistic explanation for the insensitivity of updraft velocity to SBR variations found in this and previous work (e.g., Hansen and Back, 2015). Countervailing changes in entrainment and relative humidity conspire to keep updrafts at a similar strength despite changes in cloud size and changes in diagnosed entrainment rates. Whether this cancellation of the effect of changes in entrainment and relative humidity across our simulations represents a more fundamental control of updraft speed in moist convection is a tantalising question that we hope to pursue in future work.

5 | SUMMARY AND CONCLUSIONS

This study explores the effect of two characteristic features of the land surface on the intensity of storms in idealized RCE simulations using a cloud resolving model. Simulations of high and low SBR over both homogeneous and heterogeneous surfaces are run to test the hypothesis that the high SBR and heterogeneous nature of the land surface controls the intensity of thunderstorms that form over land. It is shown from the simulations that varying the SBR over a homogeneous surface and on a surface with checkerboard pattern of varying SBR with different patch sizes does not lead to significant changes in the intensity of storms as measured by both the highest percentile in the vertical velocity and the in-cloud vertical velocity.

Consistent with the hypothesis by Williams and Stanfill (2002), a deeper boundary layer depth results in a shift toward more clouds of large spatial extent, eventually leading to differences in the distribution of entrainment, since wider clouds tend to entrain less environmental air. However, in contrast to the hypothesis and consistent with Hansen and Back (2015), the intensity of the convection does not significantly change with changing boundary layer depth. Indeed from our simulations, the cloud core vertical velocity is marginally higher in the case with shallow boundary layer depth. For the heterogeneous simulations, cloud size increases with increasing heterogeneity patch size, and therefore entrainment rate decreases with increasing patch size, but as above, this has negligible effect on measures of convective intensity such as updraft velocity.

In contrast to updraft velocity, CAPE does vary across the simulations, with the highest CAPE found in the heterogenous simulation with the smallest patch size, with CAPE systematically decreasing with increasing patch size. The disconnect between the strong variations in CAPE and the lack of variation in convective updraft velocity suggests that, consistent with previous modelling studies (e.g., Romps, 2011) undiluted cloud updrafts are virtually non-existent in our simulations.

To understand the above results, we adopted a theoretical model of convection in RCE as a spectrum of entraining plumes (Zhou and Xie, 2019). For simplicity, we limited the spectrum to only two plumes, one representing the bulk of the convective mass flux and the other representing the strongest updrafts. According to this conceptual model, the CAPE and environmental relative humidity are set by a characteristic "bulk" entrainment rate, while strong updrafts are maintained by entraining plumes with relatively low values of the entrainment rate. The magnitude of these strong updrafts are then dependent on the difference in the rate of entrainment between the bulk of convection and the strongest updrafts (Singh and O'Gorman, 2015).

According to the two-plume model, the lack of variations in updraft velocity in our simulations was a result of similar changes in the entrainment rates for the bulk of the convective mass flux and for the strongest updrafts. In addition, variations in relative humidity that offset changes the effects of a changing entrainment distribution also contributed to the insensitivity of updrafts to varying SBR and varying patch size.

While the two-plume model gives a parsimonious explanation for updraft variations among our simulations, it should be noted that it failed to account for variations in CAPE in our homogenous simulations. We speculate that this is because our measure of CAPE did not sufficiently account for differences in the properties of cloudy air parcels as they left the boundary layer that occur as the boundary layer deepens.

Our results point to a limited effect of heterogeneity and boundary-layer depth in invigorating convection in the setting of RCE. Based on our plume-spectrum model, this insensitivity of updraft strength may be partially explained by the sensitivity of the lapse rate (and therefore CAPE) in RCE to convective entrainment. In the tropics, the lapse rate is not set locally but is rapidly homogenized over large regions through the action of waves and the large-scale flow (Charney and Eliassen, 1964). This may provide a mechanism by which spatial variations in cloud entrainment, driven by spatial variations in surface properties, may be translated into more intense cloud updrafts. Exploring this

mechanism using methods to parameterize the large-scale flow (e.g., Sobel and Camargo, 2011; Kuang and Bretherton, 2006) is a possible avenue for future work.

Finally, we note that while we have examined two possible surface properties that may drive the observed land-ocean contrast in convective intensity, there are many a number of other hypotheses for the origin of this contrast that are relevant. For example, the large diurnal cycle of temperature over land compared to that of ocean has been suggested as a possible reason for enhanced convective intensity over land. However, a recent paper by Hansen *et al.* (2020) found this mechanism not to be effective in explaining the land-ocean contrast in storm intensity. Additionally, the effects of aerosols on invigorating convection have long been hypothesized to contribute to the land ocean contrast because of the higher aerosol loading over land (Williams and Stanfill, 2002; Abbott and Cronin, 2021). A comprehensive account of the factors that control the land-ocean convective intensity contrast therefore remains elusive.

acknowledgements

We acknowledge the financial support from the Australian Research Council through the Centre of Excellence for Climate Extremes (CE170100023), Grant DE190100866 and Grant DP200102954, and computational resources and services from the National Computational Infrastructure (NCI).

conflict of interest

We have no conflicts of interest to disclose.

Supporting Information

Simulation data and codes used in this work will be placed in a public repository prior to final publication.

references

Abbott, T. H. and Cronin, T. W. (2021). Aerosol invigoration of atmospheric convection through increases in humidity. *Science*, 85, 83–85. doi:10.1126/science.abc5181.

Avissar, R. and Schmidt, T. (1998). An evaluation of the scale at which ground-surface heat flux patchiness affects the convective boundary layer using large-eddy simulations. *Journal of the Atmospheric Sciences*, 55 (16), 2666–2689. doi:10.1175/1520-0469(1998)055<2666:AEOTSA>2.0.CO;2.

Bretherton, C. S., Blossey, P. N. and Khairoutdinov, M. (2005). An energy-balance analysis of deep convective self-aggregation above uniform SST. *Journal of the Atmospheric Sciences*, 62 (12), 4273–4292. doi:10.1175/JAS3614.1.

Charney, J. G. and Eliassen, A. (1964). On the Growth of the Hurricane Depression. *Journal of the Atmospheric Sciences*, 21 (1), 68–75. doi:10.1175/1520-0469(1964)021<0068:OTGOTH>2.0.CO;2.
URL http://journals.ametsoc.org/doi/10.1175/1520-0469(1964)021%3C0068:OTGOTH%3E2.0.CO;2

Christian, H. J., Blakeslee, R. J., Boccippio, D. J., Boeck, W. L., Buechler, D. E., Driscoll, K. T., Goodman, S. J., Hall, J. M., Koshak, W. J., Mach, D. M. and Stewart, M. F. (2003). Global frequency and distribution of lightning as observed from space by the Optical Transient Detector. *Journal of Geophysical Research: Atmospheres*, 108 (1). doi:10.1029/2002jd002347.

Clough, S. A., Shephard, M. W., Mlawer, E. J., Delamere, J. S., Iacono, M. J., Cady-Pereira, K., Boukabara, S. and Brown, P. D. (2005). Atmospheric radiative transfer modeling: A summary of the AER codes. *Journal of Quantitative Spectroscopy and Radiative Transfer*, 91 (2), 233–244. doi:10.1016/j.jqsrt.2004.05.058.

Giorgi, F., Avissar, R. and Brunswick, N. (1997). Representation in Earth Experience System From of H Eterogeneity Modeling ' Effects Modeling. *American Geophysical Union*, 35 (97), 413–438.

Hansen, Z. R. and Back, L. E. (2015). Higher surface Bowen ratios ineffective at increasing updraft intensity. *Geophysical Research Letters*, 42 (23), 10503–10511. doi:10.1002/2015GL066878.

Hansen, Z. R., Back, L. E. and Zhou, P. (2020). Boundary layer quasi-equilibrium limits convective intensity enhancement from the diurnal cycle in surface heating. *Journal of the Atmospheric Sciences*, 77 (1), 217–237. doi:10.1175/JAS-D-18-0346.1.

Hong, G., Heygster, G., Notholt, J. and Buehler, S. A. (2008). Interannual to diurnal variations in tropical and subtropical deep convective clouds and convective overshooting from seven years of AMSU-B measurements. *Journal of Climate*, 21 (17), 4168–4189. doi:10.1175/2008JCLI1911.1.

Kang, S. L. (2016). Regional bowen ratio controls on afternoon moist convection: A large eddy simulation study. *Journal of Geophysical Research*, 121 (23), 14,056–14,083. doi:10.1002/2016JD025567.

Kang, S.-L. and Bryan, G. H. (2011). A Large-Eddy Simulation Study of Moist Convection Initiation over Heterogeneous Surface Fluxes. *Monthly Weather Review*, 139 (9), 2901–2917. doi:10.1175/mwr-d-10-05037.1.

Khairoutdinov, M. F. and Randall, D. A. (2003). Cloud resolving modeling of the ARM summer 1997 IOP: Model formulation, results, uncertainties, and sensitivities. *Journal of the Atmospheric Sciences*, 60 (4), 607–625. doi:10.1175/1520-0469(2003)060<0607:CRMOTA>2.0.CO;2.

Knist, S., Goergen, K. and Simmer, C. (2019). Effects of land surface inhomogeneity on convection-permitting WRF simulations over central Europe. *Meteorology and Atmospheric Physics*, 132, 53–69. doi:10.1007/s00703-019-00671-y.
URL `https://doi.org/10.1007/s00703-019-00671-y`

Kuang, Z. and Bretherton, C. S. (2006). A mass-flux scheme view of a high-resolution simulation of a transition from shallow to deep cumulus convection. *Journal of the Atmospheric Sciences*, 63 (7), 1895–1909. doi:10.1175/JAS3723.1.
URL `http://journals.ametsoc.org/doi/abs/10.1175/JAS3723.1`

Lee, J. M., Zhang, Y. and Klein, S. A. (2018). The Effect of Land Surface Heterogeneity and Background Wind on Shallow Cumulus Clouds and the Transition to Deeper Convection. *Journal of the Atmospheric Sciences*, 76 (2), 401–419. doi:10.1175/jas-d-18-0196.1.

Liu, C. and Zipser, E. J. (2005). Global distribution of convection penetrating the tropical tropopause. *Journal of Geophysical Research Atmospheres*, 110 (23), 1–12. doi:10.1029/2005JD006063.

Liu, C. and Zipser, E. J. (2015). The global distribution of largest, deepest, and most intense precipitation systems. *Geophysical Research Letters*, 42 (9), 3591–3595. doi:10.1002/2015GL063776.

Liu, S., Shao, Y., Kunoth, A. and Simmer, C. (2017). Impact of surface-heterogeneity on atmosphere and land-surface interactions. *Environmental Modelling and Software*, 88, 35–47. doi:10.1016/j.envsoft.2016.11.006.
URL `http://dx.doi.org/10.1016/j.envsoft.2016.11.006`

Lucas, C., Zipser, E. J. and Lemone, M. A. (1994). Vertical Velocity in Oceanic Convection off Tropical Australia. *Journal of the Atmospheric Sciences*, 51 (21), 3183–3193. doi:10.1175/1520-0469(1994)051<3183:vvioco>2.0.co;2.

Rieck, M., Hohenegger, C. and van Heerwaarden, C. C. (2014). The Influence of Land Surface Heterogeneities on Cloud Size Development. *Monthly Weather Review*, 142 (10), 3830–3846. doi:10.1175/mwr-d-13-00354.1.

Rochetin, N., Couvreux, F. and Guichard, F. (2017). Morphology of breeze circulations induced by surface flux heterogeneities and their impact on convection initiation. *Quarterly Journal of the Royal Meteorological Society*, 143 (702). doi:10.1002/qj.2935.

Rochetin, N., Lintner, B. R., Findell, K. L., Sobel, A. H. and Gentine, P. (2014). Radiative-convective equilibrium over a land surface. *Journal of Climate*, 27 (23), 8611–8629. doi:10.1175/JCLI-D-13-00654.1.

Romps, D. M. (2011). Response of Tropical Precipitation to Global Warming. *Journal of the Atmospheric Sciences*, 68 (1), 123–138. doi:10.1175/2010JAS3542.1.
URL https://journals.ametsoc.org/doi/10.1175/2010JAS3542.1

Romps, D. M., Charn, A. B., Holzworth, R. H., Lawrence, W. E., Molinari, J. and Vollaro, D. (2018). CAPE Times P Explains Lightning Over Land But Not the Land-Ocean Contrast. *Geophysical Research Letters*, 45 (22), 12,623–12,630. doi:10.1029/2018GL080267.

Singh, M. S. and O'Gorman, P. A. (2013). Influence of entrainment on the thermal stratification in simulations of radiative-convective equilibrium. *Geophysical Research Letters*, 40 (16), 4398–4403. doi:10.1002/grl.50796.

Singh, M. S. and O'Gorman, P. A. (2015). Increases in moist-convective updraught velocities with warming in radiative-convective equilibrium. *Quarterly Journal of the Royal Meteorological Society*, 141 (692), 2828–2838. doi:10.1002/qj.2567.

Sobel, A. H. and Camargo, S. J. (2011). Projected future seasonal changes in tropical summer climate. *Journal of Climate*, 24 (2), 473–487. doi:10.1175/2010JCLI3748.1.

Williams, E., Chan, T. and Boccippio, D. (2004). Islands as miniature continents: Another look at the Land-ocean lightning contrast. *Journal of Geophysical Research D: Atmospheres*, 109 (16), 2–6. doi:10.1029/2003JD003833.

Williams, E., Mushtak, V., Rosenfeld, D., Goodman, S. and Boccippio, D. (2005). Thermodynamic conditions favorable to superlative thunderstorm updraft, mixed phase microphysics and lightning flash rate. *Atmospheric Research*, 76 (1-4), 288–306. doi:10.1016/j.atmosres.2004.11.009.

Williams, E. and Stanfill, S. (2002). The physical origin of the land–ocean contrast in lightning activity. *Comptes Rendus Physique*, 3, 1277–1292. doi:10.1016/S1631-0705(02)01407-X.

Wu, C. M., Lo, M. H., Chen, W. T. and Lu, C. T. (2015). The impacts of heterogeneous land surface fluxes on the diurnal cycle precipitation: A framework for improving the GCM representation of land-atmosphere interactions. *Journal of Geophysical Research*, 120 (9), 3714–3727. doi:10.1002/2014JD023030.

Wu, Z., Xiao, H., Lu, G. and Chen, J. (2015). Assessment of climate change effects on water resources in the yellow river basin, China. *Advances in Meteorology*, 2015, 8–12. doi:10.1155/2015/816532.

Zhou, W. and Xie, S. P. (2019). A conceptual spectral plume model for understanding tropical temperature profile and convective updraft velocities. *Journal of the Atmospheric Sciences*, 76 (9), 2801–2814. doi:10.1175/JAS-D-18-0330.1.

Zipser, E. J., Cecil, D. J., Liu, C., Nesbitt, S. W. and Yorty, D. P. (2006). Where are the most: Intense thunderstorms on Earth? *Bulletin of the American Meteorological Society*, 87 (8), 1057–1071. doi:10.1175/BAMS-87-8-1057.

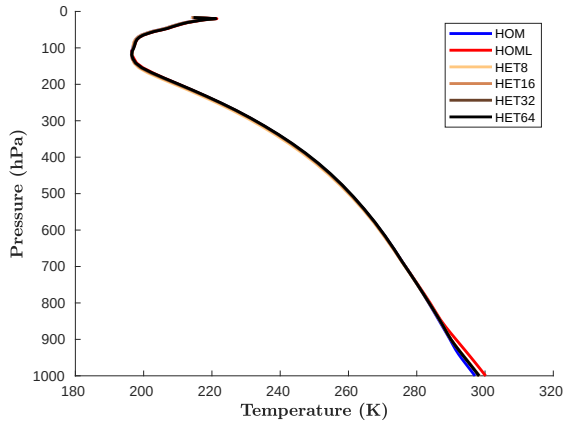

FIGURE 1 Time-and domain-mean temperature profile for homogeneous ocean-like case (HOM; blue), homogeneous land-like case (HOML; red), and heterogeneous cases with patch sizes ranging from 8 km (HET8; orange) to 64 km (HET64; black).

TABLE 1 Surface and boundary-layer properties averaged over the domain and for the last 20 days of each simulation. Boundary layer height h_{BL}, surface Bowen ratio (SBR), and relative humidity at the first model level (RH_{surf}). Boundary layer height defined as the lowest level with a non-zero cloud fraction, where cloudy grid points are taken as those with cloud water content greater than 0.01 g kg^{-1}.

Case	h_{BL} (m)	SBR	RH_{surf} (%)
HOM	598	0.09	76
HOML	1304	0.32	52
HET8	836	0.18	66
HET16	836	0.18	65
HET32	836	0.18	65
HET64	836	0.18	64

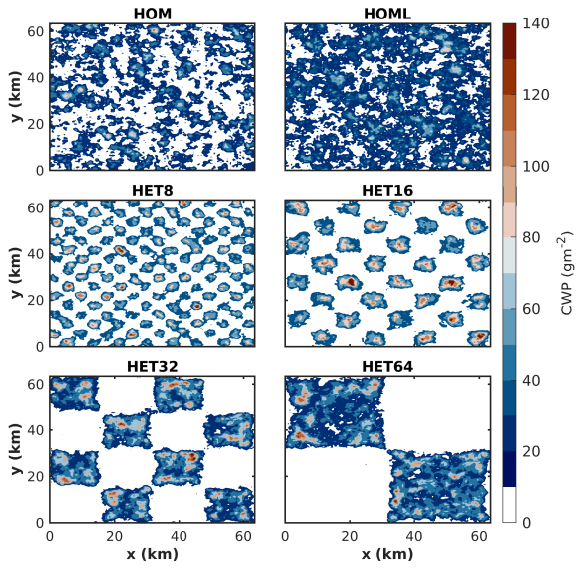

FIGURE 2 Time-mean cloud water path in each simulation. Upper row gives homogeneous ocean-like (HOM) and land-like (HOML) cases, middle and bottom row gives heterogeneous simulations with increasing patch size ranging from 8 km (HET8) to 64 km (HET64) in side length.

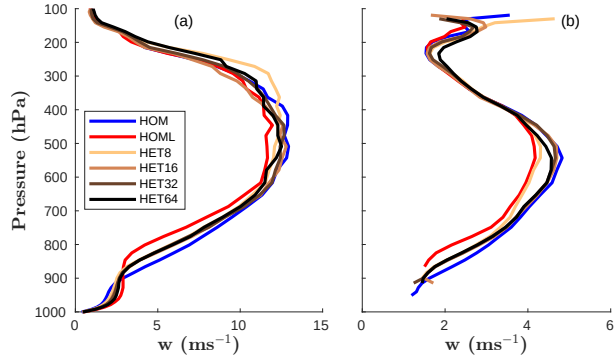

FIGURE 3 Profile of updraft velocities for homogeneous and heterogeneous simulations as given in the legend. (a) 99.99th percentile vertical velocity at each vertical level, and (b) cloud core vertical velocity at each vertical level, where cloud cores are defined as any cloudy point with vertical velocity w greater than 1 ms^{-1}.

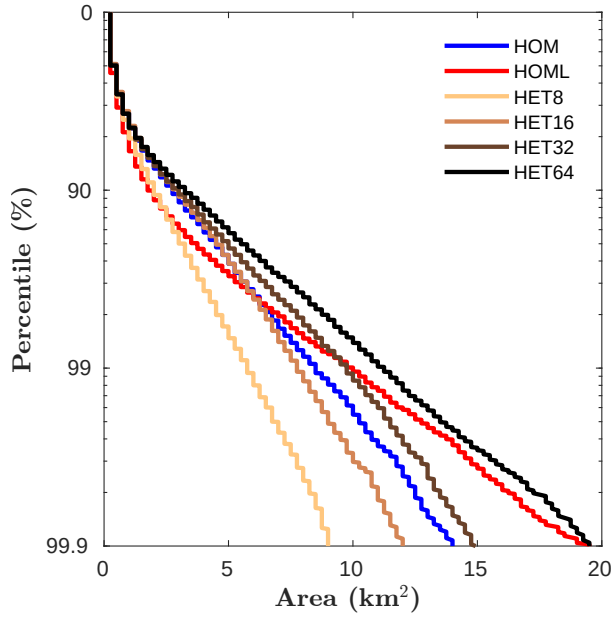

FIGURE 4 Cumulative distribution function of cloud area for levels between 2 and 5 km in height. Cloud area is calculated based on 8-connected clusters of cloudy grid points with non-precipitating condensate 0.01g kg^{-1} or greater. Cloud sizes at each model level between 2 and 5 km are considered separately and then combined to form a single distribution.

TABLE 2 Analysis of key environmental parameters from the simulations. The vertical mean relative humidity averaged between 2 to 3 km RH_{23}, the pseudoadiabatic CAPE, the entrainment rate for the bulk of the convective mass flux ϵ_{mean}, the high-percentile entrainment rate $\epsilon_{99.99}$, and scalings for the CAPE and square of the updraught velocity w^2 according to the two-plume model.

Case	RH_{23}	CAPE (kJ kg^{-1})	ϵ_{mean} (km^{-1})	$\epsilon_{99.99}$ (km^{-1})	$\epsilon_{\text{mean}}(1-RH_{23})$ (km^{-1})	$\delta\epsilon(1-RH_{23})$ (km^{-1})
HOM	0.81	1.79	0.432	0.192	0.082	0.053
HOML	0.82	1.14	0.455	0.171	0.082	0.051
HET8	0.84	1.94	0.548	0.239	0.088	0.049
HET16	0.80	1.60	0.437	0.185	0.087	0.050
HET32	0.78	1.45	0.388	0.170	0.085	0.048
HET64	0.74	1.24	0.301	0.135	0.078	0.043

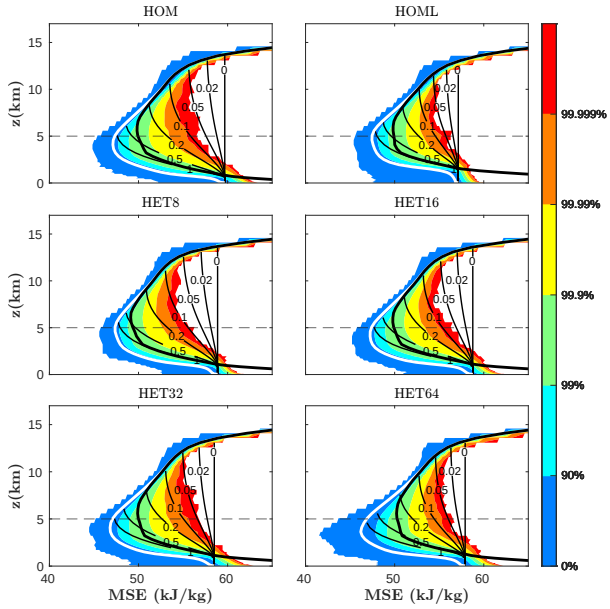

FIGURE 5 Cumulative distribution function of Moist Static Energy (MSE) at each level (colours) in the homogenous (top row) and heterogenous (middle and bottom row) simulations as labeled. White lines give domain- and time-mean MSE $\overline{h}$, thick black lines give domain- and time-mean saturated MSE $\overline{h}^*$ and thin black lines give MSE profiles h_p for plumes with entrainment rates as given by the labels in units of km^{-1} Grey dashed line marks the 5 km level.

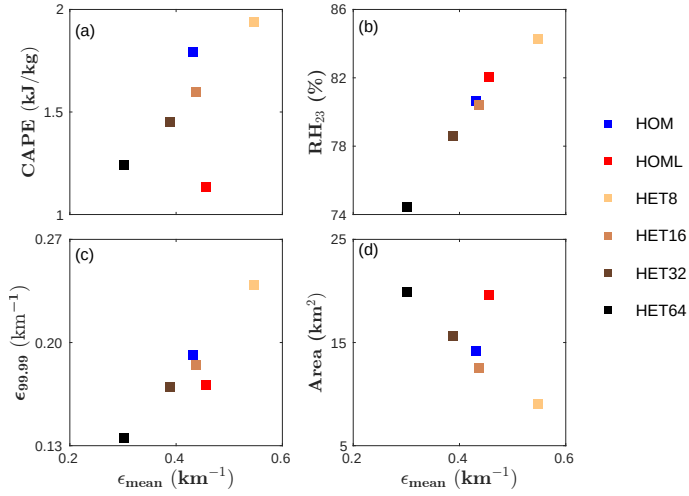

FIGURE 6 (a) CAPE, (b) Relative Humidity averaged between 2 and 3 km (RH_{23}), (c) the high-percentile entrainment rate $\epsilon_{99.99}$, and (d) the 99.9th percentile of the cloud size distribution between 2 and 5 km plotted as a function of the bulk entrainment rate ϵ_{mean}.